



OPEN ACCESS

EDITED BY

Mostafa Agour,
Aswan University, Egypt

REVIEWED BY

Nirmal Mazumder,
Manipal Academy of Higher Education,
India

Alexander Khmaladze,
University at Albany, United States
Claas Falldorf,

Bremer Institut für angewandte
Strahltechnik, Germany

André F. Müller,

Bremer Institut für angewandte
Strahltechnik, Germany, in collaboration
with reviewer CF

*CORRESPONDENCE

Frank Dubois,
✉ frank.dubois@ulb.be

RECEIVED 25 September 2023

ACCEPTED 12 December 2023

PUBLISHED 05 January 2024

CITATION

Yourassowsky C, Theunissen R,
Dohet-Eraly J and Dubois F (2024), Lipid
quantification in living microalgal cultures
with digital holographic microscopy.
Front. Photonics 4:1301708.
doi: 10.3389/fphot.2023.1301708

COPYRIGHT

© 2024 Yourassowsky, Theunissen,
Dohet-Eraly and Dubois. This is an open-
access article distributed under the terms
of the [Creative Commons Attribution
License \(CC BY\)](https://creativecommons.org/licenses/by/4.0/). The use, distribution or
reproduction in other forums is
permitted, provided the original author(s)
and the copyright owner(s) are credited
and that the original publication in this
journal is cited, in accordance with
accepted academic practice. No use,
distribution or reproduction is permitted
which does not comply with these terms.

Lipid quantification in living microalgal cultures with digital holographic microscopy

Catherine Yourassowsky, Renaud Theunissen,
Jérôme Dohet-Eraly and Frank Dubois*

Bio, Electro and Mechanical Systems, École polytechnique de Bruxelles, Université libre de Bruxelles, Brussels, Belgium

Large amounts of lipids are stored inside lipid droplets by some microalgae. Since these lipids can be used to produce nutraceuticals and biodiesel in a sustainable way, research is developing on fast non-destructive methods to quantify and monitor the amount of lipids within microalgal cultures. In this paper, we have developed with digital holographic microscopy a fast quantitative method to assess the evolution of the lipid content inside the diatom *Phaeodactylum tricornutum* living cells. The method uses a specific processing of recorded hologram sequences based on the refocusing capability in digital holographic microscopy. In representative samples of the culture, inside living cells, each lipid droplet volume is evaluated. In those experiments, for each sample, more than one thousand lipid droplets are automatically analysed from a sequence of one hundred recorded holograms. We have validated the method thanks to correlative quantitative phase contrast–fluorescence imaging and extrapolated it to larger calibrated spherical refractive particles, to demonstrate the flexibility of the method.

KEYWORDS

digital holography, microscopy, hologram processing, microalgae, lipid droplet, lipid quantification

1 Introduction

Research is increasing on microalgal lipids for nutraceutical products and for a sustainable biodiesel production (Cooper et al., 2010; Mata et al., 2010; Branco-Vieira et al., 2017; Rodolfi et al., 2017; Chia et al., 2018; Patel et al., 2019; Morales et al., 2021). Microalgae store high neutral lipid content in lipid bodies, also called lipid droplets (LDs), which can be transformed into biodiesel. Some microalgae like the diatom *Phaeodactylum tricornutum* are easy to culture, fast growing and have a fatty acid composition appropriate for biodiesel production (He et al., 2014; Branco-Vieira et al., 2017; Rodolfi et al., 2017).

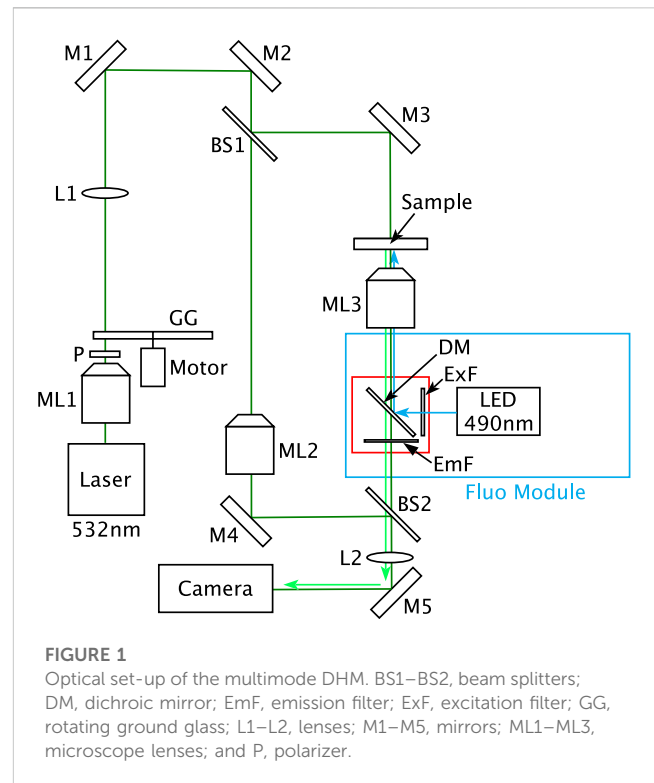
In this field, having fast non-destructive methods to quantify and monitor the amount of lipids in microalgal cultures is therefore highly important. It is particularly significant for the analysis of the best culture conditions, for the best strain selection, and for the determination of the optimal day of harvest.

The quantification of the microalgal lipid content is routinely performed by solvent extraction, gravimetric estimation, and lipid profiling with chromatography. However, these processes are destructive and the results can be distorted by a loss of lipid quantity. Moreover, they need large samples and are time-consuming (Patel et al., 2019). Fluorescent techniques like fluorescence microscopy (Mou et al., 2012; He et al., 2014;

Rumin et al., 2015; Sandmann et al., 2018) or laser scanning confocal microscopy (Wang et al., 2009; Wong and Franz, 2013) work with reduced sample amount, and allow single-cell analysis to study LDs in detail, but they are invasive by the need to stain the lipids of the cells with specific lipophilic fluorescent dyes. Moreover, those dyes present some limitations like photobleaching and variable penetration inside the cells due to the cell wall (Patel et al., 2019). Raman microscopy (He et al., 2012; Chiu et al., 2017; Patel et al., 2019) was used to perform non-destructive, label-free quantification of the lipid accumulation in microalgal cultures thanks to the detection of lipid-specific Raman spectral peaks. However, this technique is slow and invasive, as it needs a high-powered light source. The coherent anti-Stokes Raman scattering (CARS) microscopy was successfully used to visualize and quantify the microalgal LDs (He et al., 2012; Cavonius et al., 2015; Jaeger et al., 2016; Patel et al., 2019). Moreover, it allows to separate the lipid-specific signals from the excited chlorophyll fluorescence and to analyze LD formation (Jaeger et al., 2016). It is a label-free microscopy technique but it requires multiple laser sources that may affect the cell physiology, making this technique invasive (Sandmann et al., 2018).

In order to improve the monitoring of the evolution of microalgal LDs, quantitative phase contrast imaging can be performed with digital holographic microscopy (DHM), a non-invasive method that was used to assess the LDs in murine macrophage cultures (Sauvage et al., 2014). Campos et al. (2018) used DHM to perform the monitoring of adipocyte differentiation during the culture. The quantification of the lipids was monitored in the cultures thanks to the evolution of the optical path difference. Kim et al. (2016a) developed the optical diffraction tomography (ODT), able to establish the three-dimensional (3D) refractive index distribution of an individual cell from multiple two-dimensional (2D) holographic images recorded with different angles of illumination. This non-invasive method was used to perform the quantification of lipid content in hepatocytes (Kim et al., 2016b) and in individual microalgal cells (Jung et al., 2018). However, to get the information in a small field of view, it is necessary to sequentially record large amounts of holograms (usually larger than 100) having different angles of illumination. It is therefore difficult to perform the high-throughput analysis of a microalgal culture. In addition to the need of the device to create the multi-angle illumination, the observed object must remain static during the whole sequence of acquisitions, otherwise the measurements can be altered or impossible. Guo et al. (2017) developed the time-stretch quantitative phase microscopy to classify microalgal cells cultivated in two different conditions in a high-throughput way. The optical set-up is relatively complex and individual LDs are not identified.

In this paper, we develop a fast quantitative method to assess the lipid content inside the diatom *Phaeodactylum tricorutum* living cells, thanks to a specific processing of hologram sequences recorded with a DHM. This method is partly based on a previous method that we developed in 2012 with DHM to characterize spheroid transparent objects thanks to their capacity to concentrate the light, providing an intensity peak like a usual converging lens (Dubois and Yourassowsky, 2012). It is linked to the specific DHM post-recording capability of numerical refocusing, which allows the in-depth scanning of the light intensity distribution.



This method was already applied to cells in order to determine different cell features allowing, for example, the classification of living and dead cells within cultures (Dubois and Yourassowsky, 2012). Based on this method, Pirone et al. (2022) were able to detect, with a holographic flow cytometer, the alteration of the focusing property of human non-adherent cell lines due to the presence of LDs. This allowed them to distinguish a lymphocyte cell line, with a small amount of LDs, from an ovarian cancer cell line, with a high amount of LDs.

As the intracellular microalgal LDs are usually spheroid and with a higher refractive index than the external medium, we have developed the present method for the detection and the size evaluation of the LDs inside the living cells of microalgal cultures. It allows the assessment, in a non-invasive way, of the amount of lipid inside many individual living cells. This provides statistically representative data on the lipid content of the culture. We have applied it to cultures of the diatom *Phaeodactylum tricorutum*.

2 Material and methods

2.1 Optical set-up

A multimode reduced spatial coherence digital holographic microscope (DHM) is implemented to estimate the volume of LDs inside microalgal cells. As described in our patent (Dubois and Yourassowsky, 2003) and publications (Dubois et al., 2004; Dubois et al., 2011), the instrument combines the DHM with the fluorescence mode. The complete holographic information and the fluorescence signals emitted by the sample are recorded sequentially

with the same camera. This multimode DHM allows to perform correlative quantitative phase contrast–fluorescence microscopy. The overlay of the quantitative phase contrast images and the fluorescent images is a powerful tool to identify specific cells or cellular elements. In this study, it is used to identify and localize inside the algal cells the fluorescent LDs, stained with BODIPY 505/515, in the corresponding phase image and to validate the method.

The multimode DHM is schematized in Figure 1. In this instrument, the DHM is based on a Mach–Zehnder interferometer working in transmission with a partially spatially coherent illumination that is described in Dubois et al. (2006a). Thanks to this illumination the raw holograms can be directly visualized on the computer screen. Indeed, with fully coherent illumination, the direct image is usually too noisy to be interpreted by a direct viewing (Dubois et al., 1999; Dohet-Eraly et al., 2016). The spatial coherence width of the illumination, in the sample plane, was estimated at $40 \pm 5 \mu\text{m}$. It corresponds to the average size of the speckle grains observable when the ground glass (GG in Figure 1) is immobile. This size is assessed by measuring the width at half maximum of the autocorrelation of several different speckle fields.

For the DHM mode, the laser source is a Cobolt Samba™ CW 532 nm DPSSL. The microscope lenses ML2 and ML3 are oil immersion Leica 100 ×, numerical aperture (NA) 1.3, or dry Leica 40 ×, NA 0.60. The camera is a CCD camera Hamamatsu ORCA ER, with a CCD array of $1,344 \times 1,024$ pixels cropped to $1,024 \times 1,024$ pixels with a pixel size of $6.45 \mu\text{m} \times 6.45 \mu\text{m}$. The fields of view are $66 \times 66 \mu\text{m}^2$ (100 × magnification) for the LD experiments, and $171 \times 171 \mu\text{m}^2$ (40 × magnification) for the experiments on silica particles. The fluorescent light source is a CoolLED pE-100 system with a LED at 490 nm coupled with a fluorescence filter set appropriate for BODIPY 505/515.

2.2 Holograms and fluorescence signals recorded with the multimode DHM

The *Phaeodactylum tricornutum* unlabelled culture samples were injected into the micro-channel of an ibidi μ-Slide I 0.2 Luer (ibidi®) and placed on the DHM stage. Sequences of one hundred digital holograms were recorded during the translation of the DHM stage, perpendicularly to the optical axis.

For the fluorescence imaging of stained LDs, the laser source was switched off. The LED source at 490 nm was switched on for the BODIPY 505/515 fluorescence excitation and the fluorescence signals were recorded by the CCD camera. The corresponding holograms were recorded with the same camera, using the partially spatially coherent source at 532 nm while the LED source was switched off.

2.3 Culture conditions

The *Phaeodactylum tricornutum* strain (UTEX 646) was obtained from the Culture Collection of Algae at the University of Texas at Austin and was grown at 15 °C in 250 mL flasks containing 100 mL sterilized filtered seawater with 90 μL of f/2 medium (Guillard, 1975) with the salinity of 34 ppt. The

cultures were illuminated with a fluorescent lamp at $100 \mu\text{mol photons}\cdot\text{m}^{-2}\cdot\text{s}^{-1}$ on a 12:12 h light/dark cycle. To avoid bacterial contamination and for nutrient purposes, we also added 30 μL of antibiotic solution made by mixing 1 mL of purified water (milli-Q) with 35 mg of Penicillin G sodium salt and 35 mg of Streptomycin sulphate salt, 15 μL of vitamins (2.96×10^{-7} M thiamine, 2.05×10^{-9} M biotin, and 3.69×10^{-10} M cyanocobalamin), and 30 μL of silica (Na_2SiO_3) solution. Those flasks were daily shaken. The media were not changed during the cultures. Samples were taken from two separate cultures started with a delay of 3 days.

2.4 Sample preparation for fluorescence imaging

The LDs of *Phaeodactylum tricornutum* living cells were stained with the lipophilic fluorescence dye BODIPY 505/515 (Invitrogen) following the protocol described in He et al. (2014). The BODIPY 505/515 was diluted in anhydrous dimethyl sulfoxide (DMSO) to obtain a final concentration of 100 mM. 10 μL of this solution was mixed with 1 mL of the *Phaeodactylum tricornutum* culture, kept in a dark place and let settle during 5 min at room temperature (25 °C) to ensure the fluorescent labelling. The samples were injected into the micro-channel of an ibidi μ-Slide I 0.2 Luer and placed on the DHM stage.

2.5 Calibrated particles for the method validation and extrapolation

To validate the holographic method and to extrapolate it up to larger LDs as found inside adipocytes, we also tested it on calibrated monodisperse spherical silica particles of 7.82 μm diameter with a standard deviation (SD) of 0.31 μm (micro particles GmbH). As those particles are significantly larger than the LDs of *Phaeodactylum tricornutum*, we implemented in the DHM microscope objectives Leica 40 ×, NA 0.60.

2.6 Processing to compute the LD size inside the microalgal cells

In order to compute the size of the LDs inside the cells, different processing steps were applied to the recorded holograms of the culture samples. These are described in the following points.

2.6.1 Extraction of the digital holographic information

This step is achieved using the usual Fourier transform method in off-axis holography that consists in computing the discrete 2D Fourier transformation of the hologram $h_m(s, t)$, where s, t are integers ($s, t = 0, \dots, N - 1$, N being the number of pixels along one side of the hologram) and m the hologram label, isolating one of the side lobes, shifting its centre into the origin of the Fourier plane, and computing the inverse Fourier transformation. It results the complex amplitude of the object optical field $g_{0,m}(s, t)$, where the index 0 indicates that the complex amplitude is computed in the recorded plane. As previously mentioned, the holograms were

cropped to $1,024 \times 1,024$ pixels; this size was kept for all the images in the further processing.

2.6.2 Elimination of the phase and amplitude modulus artifacts

We recorded, for each sample, 100 images of the experimental slide with different lateral translation positions, in order to record representative sets of microalgal culture. Those sequences of holograms were also processed to remove the phase background and the permanent amplitude modulus defects in the images by performing averaging computations over all the recorded sequences (Yourassowsky and Dubois, 2014). After those processes, sequences of corrected complex amplitudes $g_{0,m}(s, t)$ are obtained.

2.6.3 Propagation up to the focal planes

The holograms are not necessarily recorded in the best focus plane of the microalgal cells in the sample. Therefore, it is necessary to propagate $g_{0,m}(s, t)$ up to the best focus planes of the microalgal cells by using the Fresnel diffraction equation. The propagation over a distance d is given by Nazarathy and Shamir (1980):

$$g_{d,m}(s', t') = \exp\{jkd\} F^{-1} Q[-\lambda^2 d] F^{+1} g_{0,m}(s, t) \quad (1)$$

where $s', t' = 0, \dots, N-1$ are integers, $j = \sqrt{-1}$, λ is the wavelength, $k = 2\pi/\lambda$ is the wavenumber, $F^{\pm 1}$ represent the direct (+) and inverse (-) discrete Fourier transformations and $Q[a]$ is a quadratic phase factor depending on the real parameter a :

$$Q[a] = \exp\left\{\frac{jka}{2N^2\Delta^2}(U^2 + V^2)\right\} \quad (2)$$

with Δ the sampling distance in the input plane, and U, V the discrete spatial frequencies varying from 0 to $N-1$.

According to the refocusing criteria Dubois et al. (2006b), and as the microalgal cells are mainly phase objects, the best focus distances are found by searching, for each image m , the propagation distance d for which the quantity

$$a_d = \sum_{s', t'=0}^{N-1} |g_{d,m}(s', t')| \quad (3)$$

is maximum.

In general, it is necessary to individually apply the refocusing criteria for each microalgal cell isolated within a region of interest in the complex amplitude images $g_{d,m}$ (Yourassowsky and Dubois, 2014). However, in these particular experiments, the sedimentation process located most of the microalgal cells on the bottom wall of the experimental slide in such a way that the refocusing criteria can be applied, in a very good approximation, to the full complex amplitude image $g_{d,m}$. According to the requested accuracy for the next processing step, the maximum of a_d was obtained by performing refocusing steps of $0.01 \mu\text{m}$.

As we used for the LDs $100 \times$ magnification microscope objectives, with a high numerical aperture (NA 1.3), the depth of focus (typically $0.25 \mu\text{m}$) is very small, and the lateral motions of the slide to record the sequence of images may disturb the focus. Therefore, it is necessary to perform the automated digital refocusing in each $g_{0,m}(s, t)$ as described above.

2.6.4 LD detection and diameter assessment by digital holographic propagation

The procedure for detecting and measuring individual LDs is illustrated in Figure 2, where Figure 2A shows an example of a recorded hologram. It is based on the fact that every LD may be seen as a lens, hence focusing light in a forward plane.

We assume that the refractive indices n_1 and n_2 , respectively within a droplet and outside the cell (i.e., the culture medium) are close to each other, in such a way that the paraxial approximation can be used. Indeed, in this experiment, n_1 is approximately 1.47, as vegetable oils (Jung et al., 2018), and n_2 is about 1.34 (sea water). The optical effect of the cytoplasm, which consists in a thin layer located between the LDs and the cell membrane, is weak and may therefore be ignored. Under these hypotheses, we can consider that the LD introduces a quadratic phase factor, as a usual thin lens, to an incident plane wave, which is given by Nazarathy and Shamir (1980):

$$\exp\left\{-j\frac{k}{2r}(x^2 + y^2)\right\} \quad (4)$$

where r is the light focusing distance, i.e., the focal length of the LD lens, and (x, y) are the position coordinates in the plane of the thin lens, with $(0, 0)$ in the centre of the lens. Moreover, the optical path difference emerging out of the droplet, between the centre and the border of the droplet, is $D(n_1 - n_2)$, where D is the droplet diameter. This corresponds to a phase difference of $kD(n_1 - n_2)$, which is used to adjust the parameter r in Eq. 4, as expressed by Eq. 5:

$$\begin{aligned} \exp\left\{-j\frac{k}{2r}\left[(x^2 + y^2)|_{x=0, y=0} - (x^2 + y^2)|_{x=D/2, y=0}\right]\right\} \\ = \exp\{jkD(n_1 - n_2)\} \end{aligned} \quad (5)$$

thus $(D/2)^2/2r = D(n_1 - n_2)$, which gives the r value thanks to Eq. 6:

$$r = D/[8(n_1 - n_2)] \quad (6)$$

Consequently, the light focusing distance with respect to the LD focus plane, r , is proportional to its diameter D divided by the refractive index difference.

As the exact refractive index difference is not necessarily simple to determine in practice, it can be assumed that, for a given experimental situation, it is constant. It should also be pointed out that the influence of the cytoplasm is weak. Therefore, one can model

$$br = D \quad (7)$$

where b is a constant that is experimentally determined, as explained below.

As described in 2.6.3, the complex amplitude has been first computed in the focus plane of the LDs. Then, the light focusing zone corresponding to each droplet is searched and detected by performing incremental digital reconstructions with Eq. 1. For that purpose, 120 reconstructions by steps of $0.05 \mu\text{m}$ are performed to detect the maximal local intensities. Rigorously, for every pixel, the maximal value of the intensity, among all the 120 reconstructed images, is kept. This reconstruction range and the requested sensitivity were determined after a preliminary check. In particular, the reconstruction step value has to be selected as

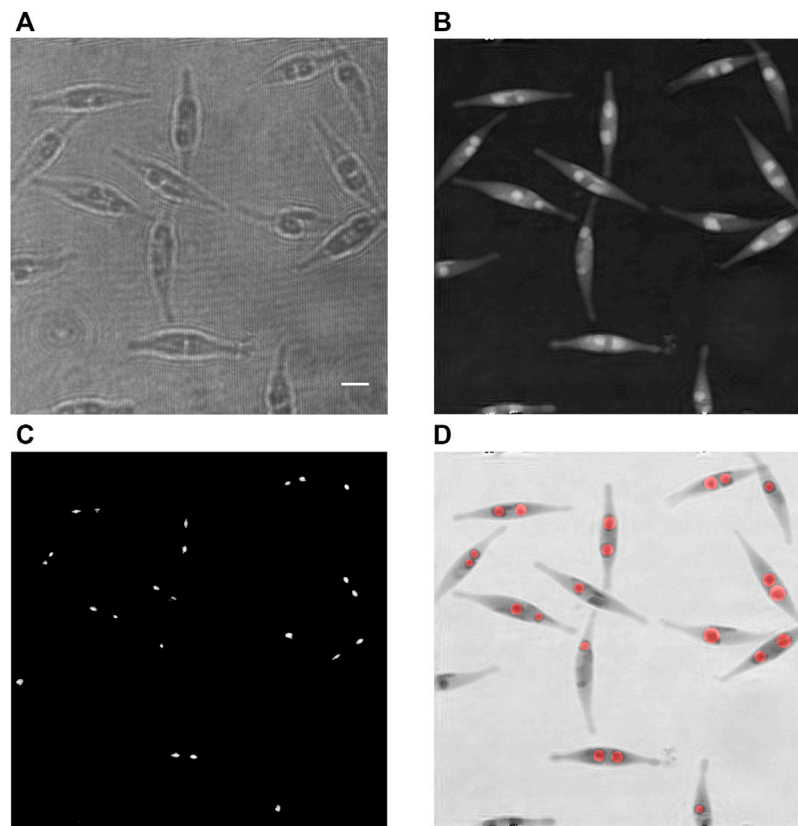


FIGURE 2

Detection and size assessment of LDs inside cells of a *Phaeodactylum tricornutum* culture at 24 days. (A) Recorded hologram; (B) corresponding refocused phase image; (C) zones of highest intensities while reconstructing over a range of 6 μm along the optical axis; each zone corresponds to one detected lipid droplet; and (D) superimposition of the inverted phase [in (B)] with the computed disks representing the assessed lipid droplets, in red; the radii of the red disks are computed according to the presented method. Scale bar = 5 μm .

smaller than the classical depth of focus, in such a way that no significant change appears between the successive reconstructions. The depth of focus in vacuum is assessed by $\lambda/2\text{NA}^2$, which corresponds to 0.16 μm in this case. A reconstruction step of 0.05 μm is therefore a suitable choice.

This process provides an image with the highest intensities while reconstructing by 6 μm along the optical axis. For each pixel, the reconstruction distance corresponding to the kept value of the intensity is stored. As the droplets are focusing the light, the intensities of each focused spot are locally significantly larger than the average intensity of the reconstructed image. Therefore, applying a threshold process to the computed image of the highest intensities allows the individual identification and segmentation of the droplets. In practice, the average image intensity and the threshold are, respectively, set to the grey levels 32 and 150 for every image (on a 256-level grey scale). The threshold operation creates small areas around the maximal focusing intensities. However, the smallest ones are not relevant as they are due to perturbations that may happen. To eliminate them, a connectivity surface analysis is performed to reject the zones having an area lesser than 20 pixels. It results a collection of the zones of interest covering the individual focusing spots generated by the LDs (Figure 2C). It has to be emphasized that the detection of the focused spots isolated by a threshold provides an efficient way to segment the droplets,

whereas the segmentation could be much more complicated in the focus plane of the LDs where they might be in contact with each other. The next step consists in searching in each zone of interest the maximal value of the intensity and to read the corresponding reconstructing distance, which gives an estimation of the light focusing distance r of the LD. Thanks to the relationship of Eq. 7, the diameter D of each LD is subsequently assessed.

In comparison with usual methods using images in the focal plane of LDs, this approach provides the huge advantage that LDs in contact give well-separated focusing spots. This is inherent to the method and largely simplifies the segmentation process of the LDs.

After this step, we dispose of a set of well-separated segmented spots, individually identifying the LDs and the corresponding diameters. An image with disks centred in each focused zone and having the computed diameters, superimposed on the respective phase image, is created to illustrate the efficiency of the developed method (Figure 2D). The aforementioned phase background correction is particularly important for this purpose, since a non-flat phase background would induce a lateral bias in the determination of the position of the LDs.

2.6.5 Parameter calibration

The determination of the b parameter of Eq. 7 is illustrated in Figure 3 and made as follows. This calibration is specific for the

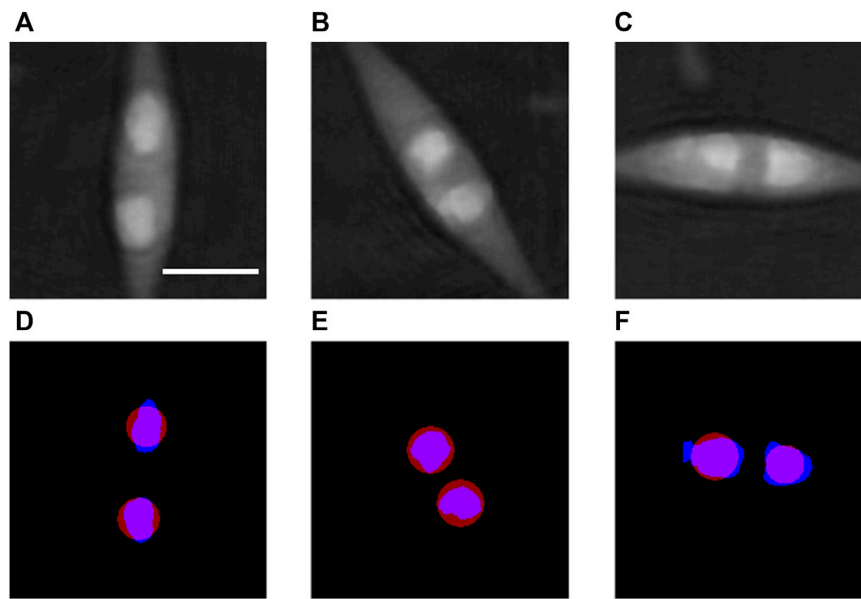


FIGURE 3

Calibration of the b parameter defined in Eq. 7. (A–C) show examples of cells from Figure 2B used for the assessment of the b parameter, with well-separated lipid droplets. (D–F) represent in blue the areas segmented with a threshold applied to the optical phase images (A–C), respectively, from which the diameter D in Eq. 7 is estimated for each droplet. The position and size of the corresponding lipid droplets obtained by the proposed method with the calibrated value of the b parameter are shown in red in (D–F). Scale bar = 5 μm .

sample type and is therefore kept for all the analyses of the same kind of samples. In a first step, we consider phase images like Figure 2B in which well-defined LDs are selected as, for instance, those in Figures 3A–C. A threshold is applied to these phase images in order to determine the areas belonging to the LDs (blue areas in Figures 3D–F). As in the correction processing described in 2.6.2 all the phase images are corrected to achieve a stable phase background, the threshold operation is very efficient. In our processing, we selected as threshold value the 150th grey level within the range of 0–255 that corresponds to the phase range $0-2\pi$. The next step consists in computing the surface area S of each selected LD and the corresponding diameter $D = 2\sqrt{S/\pi}$, assuming a circular surface.

As described in 2.6.4, the light focusing distance r is then computed for each selected LD. The b parameter is then assessed for each LD from Eq. 7: $b = D/r$. This process is applied to a set of LDs and the mean is computed. It should be added that the main goal of the proposed method is to provide a tool to study the evolution of LD sizes, which is not crucially impacted by the exact value of b , according that it must be kept identical for all the sequences of experiments.

2.6.6 Resolution limit of the method

An important aspect to determine is the smallest size of the detectable droplets. This limit finds its origin in the lateral resolution limit, which is given by $0.61\lambda/\text{NA}$ (Rayleigh criterion). Indeed, the focusing effect of the droplets imaged by digital holography is also impacted by the lateral resolution limit, by the way of a convolutional process with the point-spread function $p(x, y)$. For an in-focus input amplitude $g_0(x, y)$, the output amplitude in the detection plane can be expressed by $g_0 \otimes p$, where \otimes represents the convolution operation. This amplitude is propagated by a distance r , which corresponds to the focusing spot generated by the droplet; it results

$$R[d](g_0 \otimes p) = p \otimes R[d]g_0 \quad (8)$$

where $R[d]$ (in Eq. 8) denotes the free space propagation operator. This indicates that the focused spot is convolved by the same point spread function as the input amplitude. In order to determine what could be the minimum size of detected droplets with our method, we simulated the modification to a plane wave transmitted through a droplet of diameter D , with inside and outside refractive indices of 1.47 (lipid) and 1.34 (water), respectively. We propagated it up to the light focusing plane. We convolved the resulting amplitude with point spread functions corresponding to different NA's and we measured the ratio q between the maximum and the background intensities. We assumed that the droplet is detectable if q is larger than 3, which corresponds to a realistic threshold. We studied two cases:

- (1) D set to 3 μm and decreasing NA to get $q = 3$; we obtained NA = 0.6, which gives a ratio between D and the resolution of 5.5; and
- (2) NA set to 1.3 and decreasing D to get $q = 3$; we obtained $D = 1.2 \mu\text{m}$, which gives a ratio between D and the resolution of 4.8.

It can be concluded that the minimum size of a detected droplet is about 5 times the resolution limit. With our set-up for the LDs, that corresponds to $D = 1.25 \mu\text{m}$.

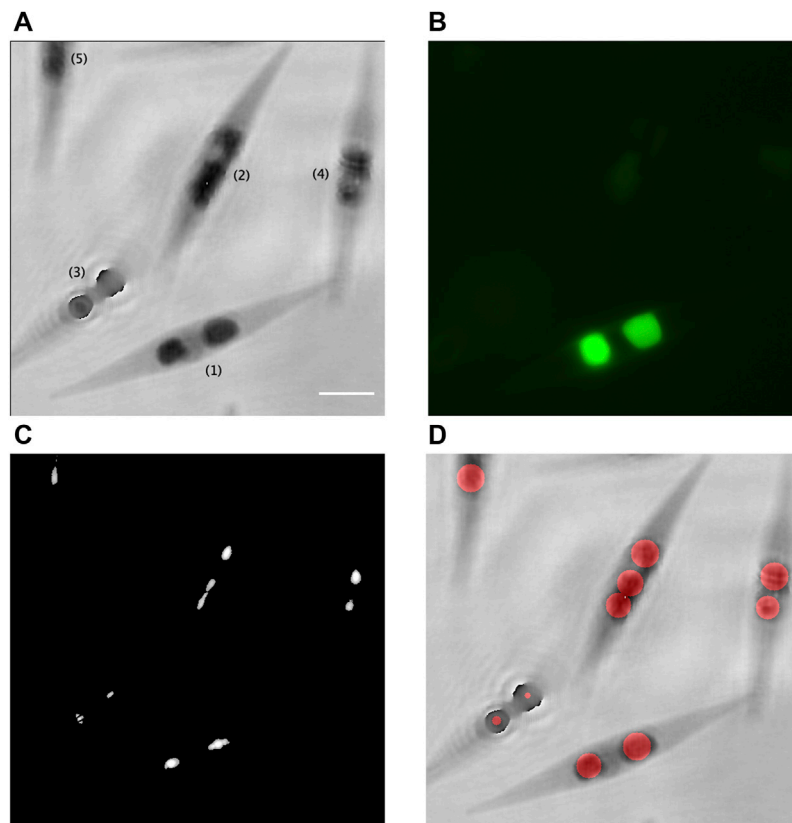
3 Results

3.1 Measurements

The results obtained on 4 series of different cultures at 24 days are given in Table 1. The number of detected LDs is relatively large that

TABLE 1 Assessment of individual LD size inside cells of 4 series of *Phaeodactylum tricornutum* cultures at 24 days.

	Number of detected LDs	LD mean volume (μm^3)	Standard deviation (μm^3)
Serie 1	1,302	4.85	3.17
Serie 2	1,422	6.28	4.02
Serie 3	2,753	5.57	3.48
Serie 4	2,667	5.56	3.65

**FIGURE 4**

Validation of the proposed method with correlative quantitative phase contrast–fluorescence imaging. (A) Inverted phase of the recorded hologram [(1), focused cell; (2), (4), and (5), slightly out-of-focus cells; and (3), largely out-of-focus cell]; (B) corresponding fluorescence image of the LDs stained with BODIPY 505/515; (C) accumulation of the zones of maximal intensities, which correspond to the intensity peaks created by the LDs; and (D) superimposition of the inverted phase of (A) with the computed disks, in red, which represent the assessed LDs. Scale bar = 5 μm .

makes the method ideal for monitoring living cell cultures by a statistically significant way. We observe that the mean values of the LD volume are in the range 4.85–6.28 μm^3 at 24 culture days that is in good agreement with the value of 5.1 μm^3 obtained by Wong and Franz (2013) with a laser scanning confocal microscope. The standard deviations are relatively important, which is also observed by Wong and Franz. It means that LD size distribution is widespread.

3.2 Validation of the method by correlative quantitative phase contrast–fluorescence imaging

The fluorescence channel of the multimode DHM allowed to validate the identification of the LDs in the phase images and the

formation of the intensity peak by each LD. Figure 4 shows an example of results on a culture at 24 days.

The size of the LDs is assessed independently with the developed method, described in 2.6, and from the fluorescence images. For the latter one, a threshold was applied to well-contrasted fluorescence images with a level of 127 with respect to the full range 0–255 to distinguish the areas belonging to the LDs from the background. Each area is then measured. The diameter of the disk having the same area is finally computed.

In Figures 4A, B, it can be seen that two in-focus fluorescent LDs stained with BODIPY 505/515 inside the cell (1) are clearly identified in the corresponding phase image. Figure 4C shows the formation of the intensity peaks by these two LDs, thanks to the numerical post-recording reconstruction in depth of the corresponding hologram. With the developed method, the

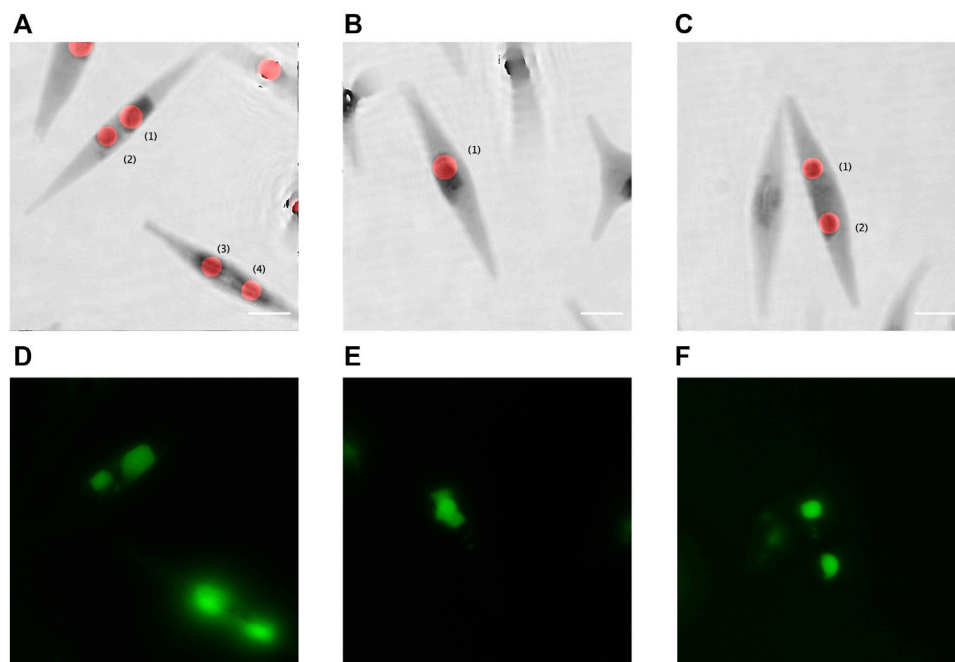


FIGURE 5

Quantitative phase contrast images, extracted from DHM, compared to the fluorescence imaging. (A–C) Inverted quantitative phase images superimposed with the red disks computed using the proposed method; and (D–F) the corresponding fluorescent images with the LDs stained with BODIPY 505/515. Scale bar = 5 μm .

computed diameter of these two LDs are estimated at 2.1 μm and 2.8 μm , as represented in red in Figure 4D, while an estimation performed on the fluorescent image gives, respectively, 2.4 μm and 3.2 μm .

In Figure 4A, the 3 cells numbered (2), (4), and (5) are slightly out of focus, which makes the LD fluorescent emission very weak. Nevertheless, we still obtained the LD focalized intensity peaks for those cells, as seen in Figure 4C, and their diameter can be evaluated with our method (Figure 4D). For the LDs inside the cell (2), we obtained three disks, possibly due to the elongated form of one of the two LDs. It provides however a good approximation of the LD total volume for this cell.

For the largely out-of-focus cell (3) in Figure 4A, the fluorescence emission is too weak to be recorded (Figure 4B). We obtained the focalized intensity peaks for this cell (Figure 4C) but the LD diameter evaluation is disturbed by their unfocused positions in

the hologram, as seen in Figure 4D. An individual refocusing of cells with the criterion in Eq. 3, as efficiently demonstrated in Yourassowsky and Dubois (2014), would allow a proper evaluation in this case.

We observed that the fluorescent emission of the BODIPY 505/515 suffers from very fast fading. Therefore, for labelled samples, it was experimentally not possible to accurately focus each fluorescent LD, record the fluorescence image, and the corresponding hologram. A few other images of fluorescent LDs are shown in Figures 5D–F. Table 2 gives a comparison of the size of the different LDs in Figure 5 measured by both holographic and fluorescent methods.

In Table 2, except for Figure 5A, LD(1), we can observe that the differences between the mean diameters obtained by the holographic and fluorescent methods are weak. Indeed, we have to compare the obtained values with the resolution limit equal to $0.61\lambda/\text{NA} \approx 0.25 \mu\text{m}$. We observe that the differences between

TABLE 2 Comparison of the measured LD sizes with the proposed holographic and the fluorescent methods.

LD identification in Figure 5	Assessed diameter–Holographic method (μm)	Assessed diameter–Fluorescent method (μm)
Figure 5A, LD (1)	2.9	3.9
Figure 5A, LD (2)	2.8	2.3
Figure 5A, LD (3)	2.4	Not measurable
Figure 5A, LD (4)	2.4	Not measurable
Figure 5B, LD (1)	2.9	2.8
Figure 5C, LD (1)	2.5	2.6
Figure 5C, LD (2)	2.5	2.4

the fluorescent and holographic methods are smaller than the resolution limit. For Figure 5A, LD(1) case, the deviation is due to the fact that this LD is highly elongated, as observed on both fluorescent and quantitative phase images, that may introduce a significant difference. However, this kind of situation has a weak impact for the establishment of statistical data to characterize LDs in a culture. We have also to point out that the fluorescent images of Figure 5A, LD(3) and Figure 5A, LD(4) cannot be measured due to the fact that they are slightly out of focus. This also constitutes a major limitation of the methods based on fluorescent imaging, which is solved by using DHM.

In conclusion, the results obtained for the in-focus fluorescent LDs confirm a correct evaluation of the LD sizes obtained with the proposed holographic method.

3.3 Validation of the method on calibrated particles

In order to validate our method for both detection and size assessment, we applied it to monodisperse silica particles having a mean diameter of $7.82\ \mu\text{m}$ (standard deviation = $0.31\ \mu\text{m}$).

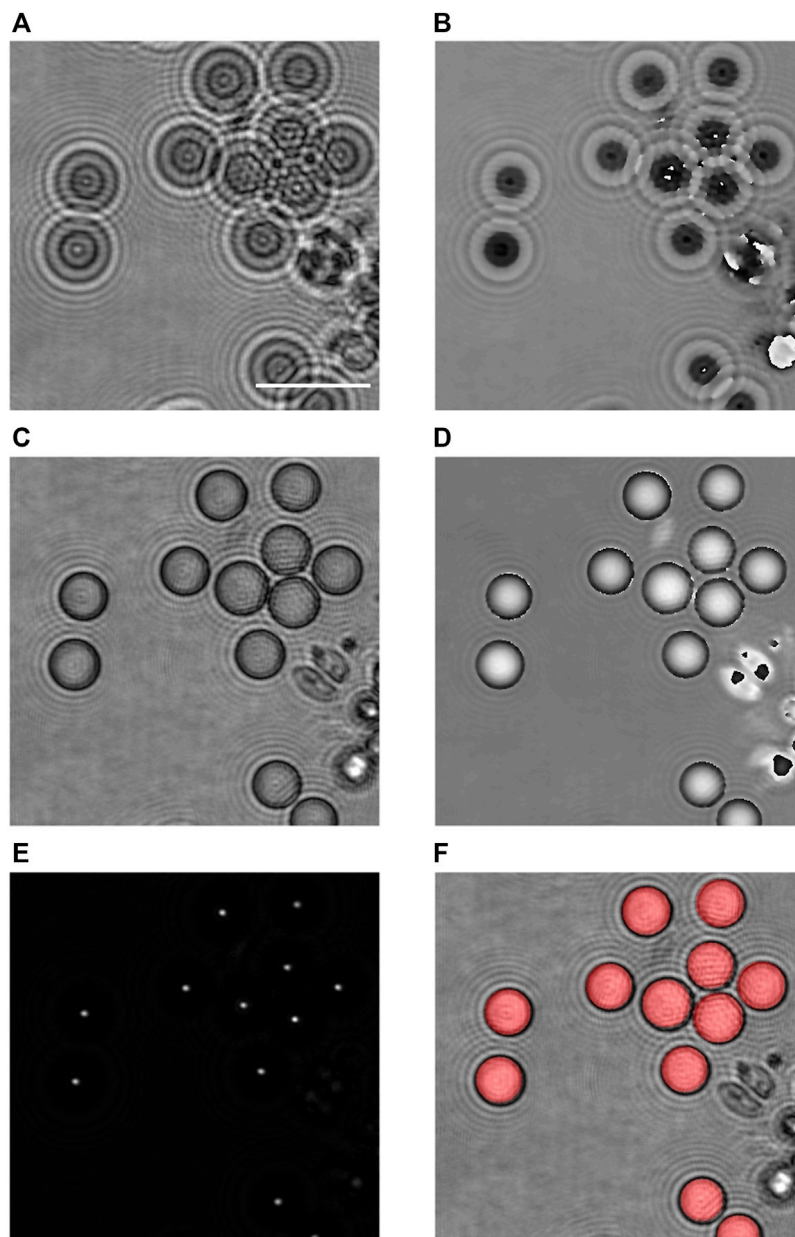


FIGURE 6

Validation of the proposed method on larger particles. (A) Amplitude modulus and (B) optical phase images of monodisperse calibrated silica particles, in the recorded plane; (C) refocused amplitude modulus and (D) optical phase; (E) reconstruction by digital holography and selection of the maximal intensities over a distance of $15.5\ \mu\text{m}$ to show the intensity peaks created by silica particles; and (F) superimposition on (C) of the disks computed according to the proposed method, in red. Scale bar = $20\ \mu\text{m}$.

Monitoring such larger particles is useful as this size can be reached for bigger LDs in other cell types such as adipocytes.

To perform the test, we prepared a suspension of these particles in water injected into an ibidi chamber. We then placed the ibidi slide in the DHM equipped with 40 ×, NA 0.60, microscope lenses. We recorded 60 images at different locations of the sample by translating the ibidi slide. The sedimented particles are recorded out of focus. The holograms are processed by the Fourier method to extract the amplitude modulus and the phase, as in the case of the LDs. Figure 6A shows an example of an extracted amplitude modulus in the recorded plane, whereas the corresponding phase is presented in Figure 6B.

The holographic complex amplitude reconstruction is applied by steps of 0.5 μm to obtain the refocused image by using Eqs 1–3, as shown in Figures 6C, D (reconstruction at −9.5 μm). As the particles are sedimented, the refocusing criterion can be applied to the full hologram field.

According to our method, the digital holographic reconstruction can then be applied in order to search and detect the maximum peak intensities of each particle (Figure 6E). As these tests are performed with 40 × microscope lenses, NA 0.60, the depth of focus is equal to $\lambda/2NA^2 = 0.74 \mu\text{m}$. The reconstruction step is therefore set to 0.5 μm. Due to the particle size dispersion, the reconstruction distance to reach the maximum intensity slightly varies for each one. We obtained an average light focusing distance r of 14 μm.

Knowing the light focusing distance r with respect to the focus plane, and measuring the diameter D in Figure 6D for several particles, it is then possible to assess the b parameter. Finally, the size of all the particles in the sequence is computed according to their own light focusing distance r , using Eq. 7 with this value of b . Figure 6F shows the superimposition on the in-focus particles, in grey, of the computed ones, in red, according to the described method. We observe that it is well superimposed.

With the proposed method, we obtained that the average diameter is 8.33 μm with a standard deviation of 0.60 μm. With the NA 0.60, the resolution limit is 0.54 μm. The difference between the supplier data and our result is 0.51 μm, which is lesser than the resolution limit. Therefore, we can conclude that our results are in good agreement with the data of the particle supplier.

It is important to outline in this example that the proposed method allows to discriminate particles that are in contact, as we can observe in Figure 6. Indeed, the focused spots by application of the digital holographic propagation (Figure 6E) are well separated, giving rise to the right identification of the particles without having to use further segmentation processes.

It is interesting to note that the method also allows the addition of complementary criteria to select the elements we want to measure. For example, it is possible to reject too small intensity peaks or to eliminate peaks that are too far with respect to the focus plane.

4 Discussion and conclusion

Thanks to DHM, we have developed a non-destructive method that allows to assess the lipid content of *Phaeodactylum tricornutum* living cell cultures in a non-invasive and fast way. As detailed in 3.1, the evaluation of the mean value of LD volume is similar to the measurement made by Wong and Franz (2013) with a laser scanning

confocal microscope on *Phaeodactylum tricornutum* in the same culture conditions.

The developed method was cross-validated thanks to the LD staining with the fluorochrome BODIPY 505/515 and the use of a multimode DHM that allows to perform correlative quantitative phase contrast–fluorescence microscopy. The method was also validated on calibrated and larger silica particles. This is meaningful as larger LDs can be found inside other cell types, as, for example, adipocytes.

Our method is validated for spherical LDs. This assumption seems acceptable, as we know that LDs tend to be spheroid objects. However, more accurate shape measurements request more sophisticated and constraining instrumentations and processes as optical diffraction tomography (Jung et al., 2018), or CARS microscopy (Cavonius et al., 2015; Jaeger et al., 2016) that make the analysis of a large number of cells more difficult. Fluorescence microscopy (Mou et al., 2012; He et al., 2014; Rumin et al., 2015; Sandmann et al., 2018) and laser scanning confocal microscopy (Wang et al., 2009; Wong and Franz, 2013) are inherently invasive and slow as there is a need to stain and to scan the sample to accurately focus each LD. Moreover there is the critical fading phenomenon for some fluorochromes as BODIPY 505/515. The proposed technique does not have such constraints and allows a non-invasive and non-destructive analysis of a large number of LDs, leading to a statistical data analysis of evolving cultures more rapidly and efficiently. This aspect is crucial with respect to the actual needs to monitor the microalgal cultures.

The method can be applied for the quantification of LDs of other microalgal species such as *Chlamydomonas* sp., *Monoraphidium neglectum*, or *Tetraselmis suecica*, for example, for which the LDs are spheroid. Even in the case of different LDs partially overlapping in the cell, the method should allow to identify the 3D localization of individual LDs inside the cell and to estimate their volume.

The method is quite effective with a short sedimentation step of the culture samples, in such a way that the refocusing of the cells can be performed in full-field images. However, it can also be used for non-sedimented and unfocused microalgal cells. In this case, each LD can be individually refocused, by using for instance the efficient method described in Yourassowsky and Dubois (2014).

In order to increase the analysis speed of the lipid microalgal cultures with the developed method, the sample can be laterally translated with a motorized stage and the holograms can be recorded with a faster camera. The microalgal culture samples could also be analysed for the lipid content in a high throughput way by the DHM that we already developed for the in-flow analysis of plankton microorganisms (Yourassowsky and Dubois, 2014). In this case, as with the proposed configuration, a full hologram is obtained for every snap shot; the hologram can be recorded very fast, with a short exposure time. In a routine configuration, one can expect an exposure time t_e of 10 μs. It is then possible to analyse flux with an acceptable maximum speed equal to the resolution ($0.61\lambda/NA$) divided by t_e , which gives $2.5 \times 10^4 \mu\text{m/s}$. Therefore, a large amount of in-flow images per second (typically 100 i/s) can be recorded, to rapidly acquire representative hologram samples of cultures, e.g., within 100 μm thickness flow cells. Moreover, most of the digital processing can be implemented on GPU to considerably reduce the processing time, to achieve fast analysis. Consequently, the reliable method described in this paper could also be implemented in an in-flow DHM, resulting in very rapidly providing the information about the lipid content of the culture.

Data availability statement

The original contributions presented in the study are included in the article, further inquiries can be directed to the corresponding author.

Author contributions

CY: Conceptualization, Data curation, Formal Analysis, Investigation, Methodology, Supervision, Validation, Visualization, Writing–original draft, Writing–review and editing. RT: Data curation, Investigation, Methodology, Validation, Writing–review and editing. JD-E: Conceptualization, Data curation, Formal Analysis, Funding acquisition, Investigation, Methodology, Software, Supervision, Validation, Visualization, Writing–original draft, Writing–review and editing. FD: Conceptualization, Data curation, Formal Analysis, Funding acquisition, Investigation, Methodology, Software, Supervision, Validation, Visualization, Writing–original draft, Writing–review and editing.

Funding

The authors declare financial support was received for the research, authorship, and/or publication of this article. During this study, JD-E was first a Postdoctoral Research Fellow of the

References

- Branco-Vieira, M., San Martin, S., Agurto, C., Santos, M. A., Freitas, M. A. V., and Caetano, N. S. (2017). Analyzing *Phaeodactylum tricornutum* lipid profile for biodiesel production. *Energy Procedia* 136, 369–373. doi:10.1016/j.egypro.2017.10.251
- Campos, V., Rappaz, B., Kuttler, F., Turcatti, G., and Naveiras, O. (2018). High-throughput, nonperturbing quantification of lipid droplets with digital holographic microscopy. *J. Lipid Res.* 59, 1301–1310. doi:10.1194/jlr.D085217
- Cavonius, L., Fink, H., Kiskis, J., Albers, E., Undeland, I., and Enejder, A. (2015). Imaging of lipids in microalgae with coherent anti-Stokes Raman scattering microscopy. *Plant Physiol.* 167, 603–616. doi:10.1104/pp.114.252197
- Chia, S. R., Ong, H. C., Chew, K. W., Show, P. L., Phang, S.-M., Ling, T. C., et al. (2018). Sustainable approaches for algae utilisation in bioenergy production. *Renew. Energy* 129, 838–852. doi:10.1016/j.renene.2017.04.001
- Chiu, L.-d., Ho, S.-H., Shimada, R., Ren, N.-Q., and Ozawa, T. (2017). Rapid *in vivo* lipid/carbohydrate quantification of single microalgal cell by Raman spectral imaging to reveal salinity-induced starch-to-lipid shift. *Biotechnol. Biofuels* 10, 9. doi:10.1186/s13068-016-0691-y
- Cooper, M. S., Hardin, W. R., Petersen, T. W., and Cattolico, R. A. (2010). Visualizing “green oil” in live algal cells. *J. Biosci. Bioeng.* 109, 198–201. doi:10.1016/j.jbiosc.2009.08.004
- Dohet-Eraly, J., Yourassowsky, C., El Mallahi, A., and Dubois, F. (2016). Quantitative assessment of noise reduction with partial spatial coherence illumination in digital holographic microscopy. *Opt. Lett.* 41, 111–114. doi:10.1364/OL.41.000111
- Dubois, F., Callens, N., Yourassowsky, C., Hoyos, M., Kurowski, P., and Monnom, O. (2006a). Digital holographic microscopy with reduced spatial coherence for three-dimensional particle flow analysis. *Appl. Opt.* 45, 864–871. doi:10.1364/ao.45.000864
- Dubois, F., Joannes, L., and Legros, J.-C. (1999). Improved three-dimensional imaging with a digital holography microscope with a source of partial spatial coherence. *Appl. Opt.* 38, 7085–7094. doi:10.1364/AO.38.007085
- Dubois, F., Schockaert, C., Callens, N., and Yourassowsky, C. (2006b). Focus plane detection criteria in digital holography microscopy by amplitude analysis. *Opt. Express* 14, 5895–5908. doi:10.1364/OE.14.005895
- Dubois, F., and Yourassowsky, C. (2003). *Method and device for obtaining a sample with three-dimensional microscopy*. U.S. Patent No 7,009,700 B2.
- Dubois, F., and Yourassowsky, C. (2012). *Optical method for characterizing transparent particles*. WO 2012/062805 A1, U.S. Patent No 9,476,694 B2.
- Dubois, F., Yourassowsky, C., Callens, N., Minetti, C., Queeckers, P., Podgorski, T., et al. (2011). “Digital holographic microscopy working with a partially spatial coherent source,” in *Coherent light microscopy, imaging and quantitative phase analysis*. Editors P. Ferraro, A. Wax, and Z. Zalevsky (Berlin, Germany: Springer), 31–59. doi:10.1007/978-3-642-15813-1
- Dubois, F., Yourassowsky, C., and Monnom, O. (2004). “Microscopie en holographie digitale avec une source partiellement cohérente,” in *Imagerie et Photonique pour les Sciences du Vivant et de la Médecine*. Editors M. Faupel, P. Smigielski, and R. Grzymala (Lüdenscheid, Nordrhein-Westfalen: Fontis Media), 287–302.
- Guillard, R. R. L. (1975). “Culture of phytoplankton for feeding marine invertebrates,” in *Culture of marine invertebrates animals*. Editors W. L. Smith and M. H. Chanley (New York: Plenum Press), 29–60. doi:10.1007/978-1-4615-8714-9-3
- Guo, B., Lei, C., Kobayashi, H., Ito, T., Yalikul, Y., Jiang, Y., et al. (2017). High-throughput, label-free, single-cell, microalgal lipid screening by machine-learning-equipped optofluidic time-stretch quantitative phase microscopy. *Cytom. A* 91, 494–502. doi:10.1002/cyto.a.23084
- He, L., Han, X., and Yu, Z. (2014). A rare *Phaeodactylum tricornutum* cruciform morphotype: culture conditions, transformation and unique fatty acid characteristics. *PLoS One* 9, e93922. doi:10.1371/journal.pone.0093922
- He, X. N., Allen, J., Black, P. N., Baldacchini, T., Huang, X., Huang, H., et al. (2012). Coherent anti-Stokes Raman scattering and spontaneous Raman spectroscopy and microscopy of microalgae with nitrogen depletion. *Biomed. Opt. Express* 3, 2896–2906. doi:10.1364/BOE.3.002896
- Jaeger, D., Pilger, C., Hachmeister, H., Oberländer, E., Wördenweber, R., Wichmann, J., et al. (2016). Label-free *in vivo* analysis of intracellular lipid droplets in the oleaginous microalga *Monoraphidium neglectum* by coherent Raman scattering microscopy. *Sci. Rep.* 6, 35340. doi:10.1038/srep35340
- Jung, J., Hong, S.-J., Kim, H.-B., Kim, G., Lee, M., Shin, S., et al. (2018). Label-free non-invasive quantitative measurement of lipid contents in individual microalgal cells using refractive index tomography. *Sci. Rep.* 8, 6524. doi:10.1038/s41598-018-24393-0
- Kim, K., Lee, S., Yoon, J., Heo, J., Choi, C., and Park, Y. (2016b). Three-dimensional label-free imaging and quantification of lipid droplets in live hepatocytes. *Sci. Rep.* 6, 36815. doi:10.1038/srep36815
- Kim, K., Yoon, J., Shin, S., Lee, S., Yang, S.-A., and Park, Y. (2016a). Optical diffraction tomography techniques for the study of cell pathophysiology. *J. Biomed. Photonics Eng.* 2, 020201-1–020201-16. doi:10.18287/JBPE16.02.020201

Fondation Philippe Wiener–Maurice Anspach and then Chargé de Recherches du Fonds de la Recherche Scientifique–FNRS.

Acknowledgments

The authors acknowledge Nathalie Gypens, Boris Wittek, and Colin Royer of the Laboratoire d’Écologie des Systèmes aquatiques de l’Université libre de Bruxelles for their support for the *Phaeodactylum tricornutum* culture.

Conflict of interest

The authors declare that the research was conducted in the absence of any commercial or financial relationships that could be construed as a potential conflict of interest.

Publisher’s note

All claims expressed in this article are solely those of the authors and do not necessarily represent those of their affiliated organizations, or those of the publisher, the editors and the reviewers. Any product that may be evaluated in this article, or claim that may be made by its manufacturer, is not guaranteed or endorsed by the publisher.

- Mata, T. M., Martins, A. A., and Caetano, N. S. (2010). Microalgae for biodiesel production and other applications: a review. *Renew. Sustain. Energy Rev.* 14, 217–232. doi:10.1016/j.rser.2009.07.020
- Morales, M., Aflalo, C., and Bernard, O. (2021). Microalgal lipids: a review of lipids potential and quantification for 95 phytoplankton species. *Biomass Bioenergy* 150, 106108. doi:10.1016/j.biombioe.2021.106108
- Mou, S., Xu, D., Ye, N., Zhang, X., Liang, C., Liang, Q., et al. (2012). Rapid estimation of lipid content in an Antarctic ice alga (*Chlamydomonas* sp.) using the lipophilic fluorescent dye BODIPY_{505/515}. *J. Appl. Phycol.* 24, 1169–1176. doi:10.1007/s10811-011-9746-4
- Nazarathy, M., and Shamir, J. (1980). Fourier optics described by operator algebra. *J. Opt. Soc. Am.* 70, 150–159. doi:10.1364/JOSA.70.000150
- Patel, A., Antonopoulou, I., Enman, J., Rova, U., Christakopoulos, P., and Matsakas, L. (2019). Lipids detection and quantification in oleaginous microorganisms: an overview of the current state of the art. *BMC Chem. Eng.* 1, 13. doi:10.1186/s42480-019-0013-9
- Pirone, D., Sirico, D. G., Mugnano, M., Del Giudice, D., Kurelac, I., Cavina, B., et al. (2022). Finding intracellular lipid droplets from the single-cell biolens' signature in a holographic flow-cytometry assay. *Biomed. Opt. Express* 13, 5585–5598. doi:10.1364/BOE.460204
- Rodolfi, L., Biondi, N., Guccione, A., Bassi, N., D'Ottavio, M., Arganaraz, G., et al. (2017). Oil and eicosapentaenoic acid production by the diatom *Phaeodactylum tricorutum* cultivated outdoors in green wall panel (GWP[®]) reactors. *Biotechnol. Bioeng.* 114, 2204–2210. doi:10.1002/bit.26353
- Rumin, J., Bonnefond, H., Saint-Jean, B., Rouxel, C., Sciandra, A., Bernard, O., et al. (2015). The use of fluorescent Nile red and BODIPY for lipid measurement in microalgae. *Biotechnol. Biofuels* 8, 42. doi:10.1186/s13068-015-0220-4
- Sandmann, M., Schafberg, M., Lippold, M., and Rohn, S. (2018). Analysis of population structures of the microalga *Acutodesmus obliquus* during lipid production using multi-dimensional single-cell analysis. *Sci. Rep.* 8, 6242. doi:10.1038/s41598-018-24638-y
- Sauvage, A., Dubois, F., Haumont, D., Pireaux, V., El Mallahi, A., Yourassowsky, C., et al. (2014). "Evaluation of lipid loading in macrophages using Digital Holographic Microscopy (DHM): a new non-invasive and quantitative technology," in Proceedings of the Presented at the 28th annual conference of the European Macrophage and Dendritic Cell Society, Vienna, Austria, October 2014, 2–4.
- Wang, Z. T., Ullrich, N., Joo, S., Waffenschmidt, S., and Goodenough, U. (2009). Algal lipid bodies: stress induction, purification, and biochemical characterization in wild-type and starchless *Chlamydomonas reinhardtii*. *Eukaryot. Cell* 8, 1856–1868. doi:10.1128/EC.00272-09
- Wong, D. M., and Franz, A. K. (2013). A comparison of lipid storage in *Phaeodactylum tricorutum* and *Tetraselmis suecica* using laser scanning confocal microscopy. *J. Microbiol. Methods* 95, 122–128. doi:10.1016/j.mimet.2013.07.026
- Yourassowsky, C., and Dubois, F. (2014). High throughput holographic imaging-in-flow for the analysis of a wide plankton size range. *Opt. Express* 22, 6661–6673. doi:10.1364/OE.22.006661